Reactivating and Calming Volcanoes: The 2015 M W 8.3 Illapel Megathrust Strike

Article *in* Geophysical Research Letters · August 2020

DOI: 10.1029/2020GL087738

CITATIONS
23

READS
399

2 authors:

Cristian Farias
Temuco Catholic University
25 PUBLICATIONS **143** CITATIONS
SEE PROFILE

Daniel Basualto
Universidad de La Frontera
38 PUBLICATIONS **286** CITATIONS
SEE PROFILE

Geophysical Research Letters

RESEARCH LETTER
10.1029/2020GL087738

Reactivating and Calming Volcanoes: The 2015 M_W 8.3 Illapel Megathrust Strike

Cristian Farías[1] and Daniel Basualto[2,3]

[1]Departamento de Geología y Obras Civiles, Universidad Católica de Temuco, Temuco, Chile, [2]Departamento de Ingeniería en Obras Civiles, Facultad de Ingeniería y Ciencias, Universidad de la Frontera, Temuco, Chile, [3]Escuela de Geología, Facultad de Ciencias, Universidad Austral de Chile, Valdivia, Chile

Key Points:
- The 2015 M_W 8.3 Illapel earthquake was followed by very different responses from Nevados de Chillán, Copahue, and Villarrica volcanoes
- Two volcanoes were reactivated and another one was shut down by the megathrust earthquake
- Seismic waves altered the local fault systems dynamically, which then served as pathways for fluids to move

Supporting Information:
- Supporting Information S1

Correspondence to:
C. Farías,
cristian.farias@uct.cl

Citation:
Farías, C., Basualto, D. (2020). Reactivating and calming volcanoes: The 2015 M_W 8.3 Illapel megathrust strike. *Geophysical Research Letters*, *47*, e2020GL087738. https://doi.org/10.1029/2020GL087738

Received 3 MAR 2020
Accepted 12 JUL 2020
Accepted article online 17 JUL 2020

Abstract The 2015 M_W 8.3 Illapel earthquake was followed in a time frame of weeks to months by very different responses from Nevados de Chillán, Copahue, and Villarrica volcanoes, all located more than 580 km from the rupture zone. Here we show how Nevados de Chillán and Copahue started new eruptive phases, and Villarrica entered in a period of relative calm. Using seismic, geodetic, and geochemical observations, in combination with numerical wave propagation simulations, we also show that the geometry of the fault system controlled the impact of the earthquake on each volcano. We argue that the sensitivity of a volcano toward an earthquake depends on both its critical state before the mainshock and the geometry of its fault system. This is a case where the same earthquake generates very different responses at the same time, at large distances, rendering volcanoes as very sensitive systems.

Plain Language Summary Earthquakes can affect volcanoes in a wide range of distances and time windows. Most of the literature has focused on the cases where episodes of volcanic unrest (including eruptions) follow earthquakes, with very few cases of periods of calm being reported as responses to a seismic event. On 16 September 2015, a large M_W 8.3 megathrust shook central Chile and was followed by very different responses from three volcanoes located more than 580 km away. They were Nevados de Chillán, Copahue, and Villarrica. Both Nevados de Chillán and Copahue erupted within weeks and months following the megathrust, but Villarrica entered in a period of relative calm. This contrast in the responses from volcanic systems to the same large earthquake has not been reported before. We also performed numerical simulations to analyze the impact of the seismic waves on each system. We found out that the geometry of the underlying fault systems that serve as fluid motion pathways at each volcano controls the way an earthquake can affect them, even at large distances, which renders volcanoes as very sensitive systems.

1. Introduction

Most of continental Chile is dominated by the fast oblique subduction between the Nazca and South American plates, which converge with a mean speed of ~66 mm/year. The M_W 8.3 2015 Illapel event occurred in what was a highly locked zone (Métois et al., 2012; Ruiz & Madariaga, 2018), as part of a large sequence of strong earthquakes (1880, 1943, and 2015), which have partially unlocked the northern section of the 1730 M_W 9.1–9.2 megathrust earthquake rupture zone. The earthquake had a 200 km long rupture zone with a maximum slip in the order of 8 m (Heidarzadeh et al., 2015; Ruiz et al., 2016; Satake & Heidarzadeh, 2017; USGS, 2015). Nineteen volcanoes in the Central-South Chile Volcanic Zone (CSCVZ, considered here from −33° to −40°) were under monitoring by the Chilean Volcano Observatory (OVDAS). Three of them followed the mainshock with changes on their activities during a period of several weeks. They were Nevados de Chillán (NdC), Copahue (COP), and Villarrica (VIL), located 581, 692, and 863 km away from the earthquake hypocenter, respectively. These volcanoes are located in a very active geological setting, where the right-lateral strike-slip Liquie-Ofqui Fault System (LOFS; Pliocen/Holocene) and NW Andean Transverse Faults (Paleozoic/Triassic) are important geological features (Legrand et al., 2011; Sánchez et al., 2013), whose activity also has a large influence on the CSCVZ (Catalán et al., 2017; Cembrano & Lara, 2009; Cembrano et al., 1996; Stanton-Yonge et al., 2016; Tardani et al., 2016). Figure 1 shows the geometry of the main fault systems for each volcano, based on several descriptions (Bonali et al., 2016; Cardona et al., 2018; Gonzalez-Ferrán, 1995; Melnick et al., 2006; Meulle-Stef et al., 2016; Moreno & Clavero, 2006), and also shows the rupture zones of the most recent historical earthquakes in the region

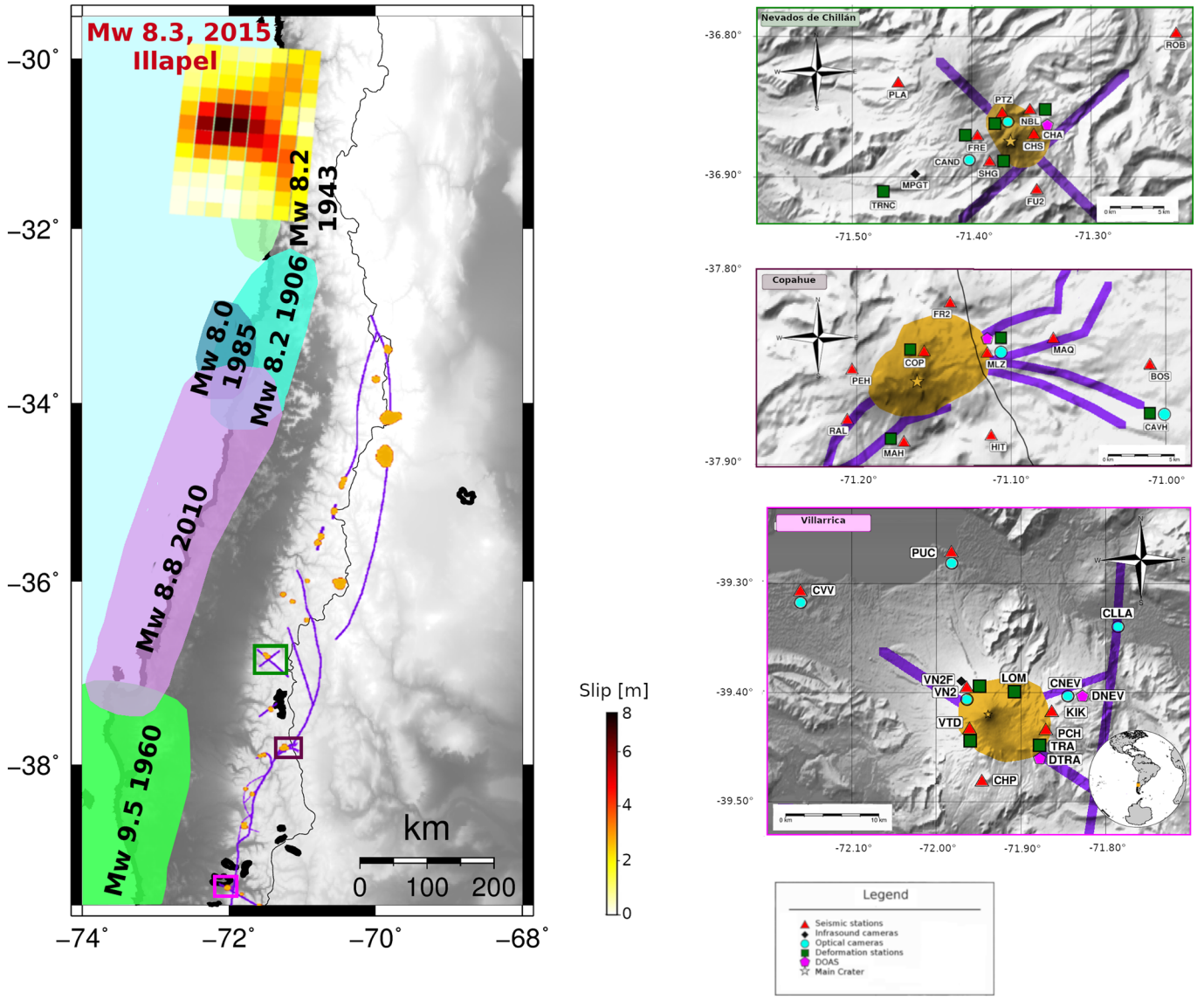

Figure 1. Left panel: Chile map, including the 2015 M_W 8.3 Illapel earthquake slip distribution from Heidarzadeh et al. (2015), a sketch of the main fault systems and inferred fluid reservoirs for the different volcanoes, and the rupture zones of the 1906, 1943, 1960, 1985, and 2010 earthquakes. Right panels: Zoom to Nevados de Chillán (top), Copahue (middle), and Villarrica (bottom), showing OVDAS station distribution, as well as a sketch of the main faults (in purple) and fluid reservoirs (in orange) for each one of them at h= 3,000 m depth.

(Ruiz & Madariaga, 2018). Some of them have been followed by eruptions at NdC, COP, and VIL up to 2 years after their occurrence date (Bonali, 2013; Farías et al., 2014; Watt et al., 2009). Following the findings of Farías et al. (2017) and Farías and Galván (2020), we argue that the geometry of each main fault system of a volcano helps to control the influence of external earthquakes on them. We studied the seismic, geodetic, and geochemical observations of all the volcanoes of the CSCVZ, obtained from OVDAS and performed wave propagation numerical simulations in order to better assess the influence of the Illapel megathrust on the CSCVZ.

2. Data and Methods

2.1. Data and Volcano Monitoring Routines and Networks Used by OVDAS

To account for the changes on the dynamics of each one of the three volcanoes studied here, we used data from the monitoring network of OVDAS (Figures 1 and S1 in the supporting information). The network

involves several seismic, GPS, and Differential Optical Absorption Spectrometer (DOAS) stations, as well as optical cameras. Data presented and analyzed in this article was recorded in a time window of 1 year, from February 2015 to January 2016. OVDAS personnel identified individual seismic events from the continuous signal and extracted the basic information for each of them. The HYPO71 routine was used to obtain the hypocentral location of the Volcano-tectonic (VT) events (Bachmann et al., 2012; Wassermann, 2012). The size of Long Period (LP) (Kumagai & Chouet, 1999; McNutt, 2005) and Very Long Period (VLP) events was obtained by calculating the reduced displacement (D_R) (Aki, 1981). To monitor the seismic activity in real time, both the RSAM (Real-time Seismic Amplitude Measurement; Endo & Murray, 1991) and SSAM (Real-time Seismic Spectral Amplitude Measurement; Rogers & Stephens, 1995) analysis tools were used.

To measure the SO_2 concentration at Copahue volcano, OVDAS used a mini-DOAS station called "Mellizas" (MLZ in Figure S1), which is located 5 km east-northeast (ENE) of Copahue volcano summit, in the direction of prevailing winds. This station operated during the daylight, taking scans between 3 and 14 min, depending on light intensity, producing a total of 50 to 140 per day. Data were evaluated and processed by the NOVAC software.

We also used data from the five continuous double-frequency geodesic GNSS stations installed around Villarrica volcano. Data were recorded every 15 s in 24 hr files. Postprocessing was carried out by Trimble 4-D Control software, considering a 10° elevation mask over the horizontal, a minimum of four satellites in simultaneous common registration for each point, using ephemerides released with 2 weeks of lag, for accurate processing data. This methodology allows location accuracy in the order of 2 mm in the horizontal position and 5 mm in the vertical position for each calculated point. We only used the VN2-TRL line (Figure S1) because this pair of GPS stations showed the clearest deformation in this period of time.

2.2. Details on the Implementation of the Numerical Simulations

To be able to tell whether the changes in volcanic activity by NdC, COP, and VIL, can be linked to the Illapel earthquake, we analyzed the plausible physical mechanisms which could have altered them. Due to the large distance between the earthquake and the volcanic centers, the permanent change in static stress is negligible (lower than 100 Pa) at the volcanoes under study here (Bonali, 2013; Bonali et al., 2013; Farías et al., 2017; Walter, 2007; Walter & Amelung, 2007), so we focused on the dynamic influence of the megathrust in the stress tensor, energy density, and in the dynamics of the local fault systems. We carried out 2-D wave propagation numerical simulations, using the method of Farías et al. (2017), where we consider the fluid reservoirs of each one of the volcanic systems and their fault systems as places with different elastic parameters. We simulated the seismic wave propagation due to the Illapel earthquake in the chilean backarc using a 2-D fluid-saturated x-y poroelastic domain buried at $h = 3{,}000$ m, for computational efficiency. We used a $2{,}500 \times 2{,}500$ km plane, which includes the $525 \times 1{,}050$ km area of interest inside. Figures 1 and S1 show an schematic view of the main features of our domain, including a sketch of the main structures, the reference frame, and the rupture region of the Illapel megathrust event from Heidarzadeh et al. (2015). Because of our 2-D modeling, we assumed faults to continue vertically up to at least h. We used an explicit finite-differences scheme following the method of Farías et al. (2017), with a spacing between neighboring points in the grid of 1 km. The domain was larger to prevent artificial wave reflections at the boundaries, after using the Convolutional Perfect Matched Layer technique (Farías et al., 2017; Martin et al., 2008) to dampen the perturbations first.

We coupled the seismic wave-induced changes in the stress tensor due to the Illapel megathrust with fluid dynamics in order to follow the short-term interaction between stress transfer and fluid motion. Following the method of Farías et al. (2017), we considered a fluid-saturated poroelastic domain to perform each simulation. Due to our reference frame election, we used the convention that compression is negative. To generate the Illapel earthquake in a 2-D domain, we started from the source slip distribution published by Heidarzadeh et al. (2015). We then used the equations by Okada (1992) to calculate the displacements produced by the megathrust in an x-y plane buried at $h = 3{,}000$ m depth. Afterward, we took the projection of the rupture area into this displacement field, and we moved each point of this section, to produce the seismic waves, following a temporal displacement function based on the work of Bizzarri (2012). Due to the 2-D nature of our domain, this procedure generates only body waves. We also simulated a Rayleigh wave with a period of about 20 s, which is consistent with the waveforms of the earthquake recorded at NdC and COP (data from VIL was temporary lost during the earthquake; see supporting information), and then we added the

contributions from body and surface waves to obtain the displacement and velocity fields. We then followed the changes in stresses, velocities, displacements, energy density, and fluid overpressure, in time and space. Table S1 shows all parameters we used, based on the definitions of the Farías et al. (2017) model equations.

3. Results

3.1. Preseismic State of the Volcanoes in the CSCVZ

Only NdC, COP, and VIL showed signs of unrest in the CSCVZ in a time frame of several months and weeks prior to the 2015 Illapel megathrust. NdC had an unusual rate of VT seismicity several times during 2015 (Figures 2 and S4), and a slight increase in LP activity about 2 weeks before the Illapel earthquake, evidencing a system with activity slightly higher than usual. COP volcano was in the midst of several minor eruptive phases, which started on 22 December 2012 (Venzke, 2020), being in an altered state before the earthquake. Figure S12 shows its alert levels from September 2014, to September 2016. Notice that not all eruptions are accompanied by a red alert level (see the supporting information for more details). An increase in VLP seismicity and SO_2 degassing activity 2 weeks before the mainshock (Figures 2 and S5) suggest that most of COP activity came from the internal fluid dynamics of the volcano before the waves arrived. The open-conduit VIL volcano had a brief eruption on 3 March 2015, which lasted less than a day (Johnson & Palma, 2015; Venzke, 2020). GPS observations (Figures 2 and S6) show active deformation in the following months, which has been linked to a posteruptive episode of magma intrusion from depth (Córdova et al., 2015). There was also a slight increase on LP activity before the Illapel earthquake, which was accompanied by a boost on the RSAM (Figures 2 and S6). Another volcano that had anomalous seismicity before the megathrust onset was Laguna del Maule, which showed seismic swarms in April and August 2015 (Figure S12), which seems to be linked to the rapid uplift that has been recorded on the volcanic complex since 2011, as reported by Cardona et al. (2018), and not to a period of increased volcanic activity before the earthquake.

3.2. Response of the Volcanoes in the CSCVZ

The activities of NdC, COP, and VIL volcanoes suffered important changes following the Illapel earthquake. The coseismic unrest at NdC, evidenced by a stark change in the dominant frequencies of the SSAM, is mostly linked to fluid activity, since there is no apparent increase in VT seismicity in the weeks following the mainshock (Figure S8). This is consistent with the change in the Reduced Displacement (Aki, 1981) after the Illapel earthquake (Figure S4). The volcano then exhibited a second stage of unrest, which led to the beginning of an eruptive phase in January 2016. The explosions during 2016 and 2017 were mostly phreatic (Luengo et al., 2017), indicating that the main source of unrest comes from the excitation of the large hydrothermal field of the complex. Magma arrived into the surface when a fissure was open on top of the erupting crater (OVDAS-Sernageomin, 2017). Since then, a dacitic lava dome has been growing on top of the fissure, accompanied by small explosions, pyroclastic flows, nocturnal incandescence, and even a lava flow (OVDAS-Sernageomin, 2018, 2019). COP volcano followed the megathrust with two M_l 2.8 and M_l 3.3 VT events, which occurred beneath the volcano main crater immediately after the arrival of the Illapel earthquake seismic waves (OVDAS-Sernageomin, 2015). This was followed by an important VT swarm on a nearby, north trending fault, that lasted for 17 days (Figures 2, S5, and S9). Afterward, a new eruptive phase began, fueled by new andesitic magma, ending on 30 December 2016. VIL exhibited an immediate increase in VT activity in an apparent second-order NE striking fault and a boost on LP event rate, which lasted for a week and a half (Figures 2, S6, and S10), following the earthquake. There was also an noticeable occurrence of high-frequency LP events, evidenced by changes in SSAM (Figure S6). There was also a change in the deformation rate of the volcano. Its posteruptive inflationary process ended 2 weeks before the Illapel earthquake, entering in a short-lived metastable phase. A deflationary process was evident after the megathrust and stopped in November 2015, with the volcano entering in a period of relative stability after that (Figure S6). Therefore, we link VIL LP activity boost to the influence of the Illapel earthquake in the shallow fluids that were already present at the volcano once the earthquake occurred, and not to new magma coming from depth. Two other volcanoes from the CSCVZ did show an increase on their activities in the months following the earthquake (Figure S12), but we do not have evidence to associate them to the influence of the seismic event. They were Laguna del Maule and Planchón-Peteroa. The former showed two more seismic swarms in November and December 2015 in the same region as the ones that occurred sporadically since 2011 (Cardona et al., 2018). The latter showed a significant boost in LP activity, which was accompanied

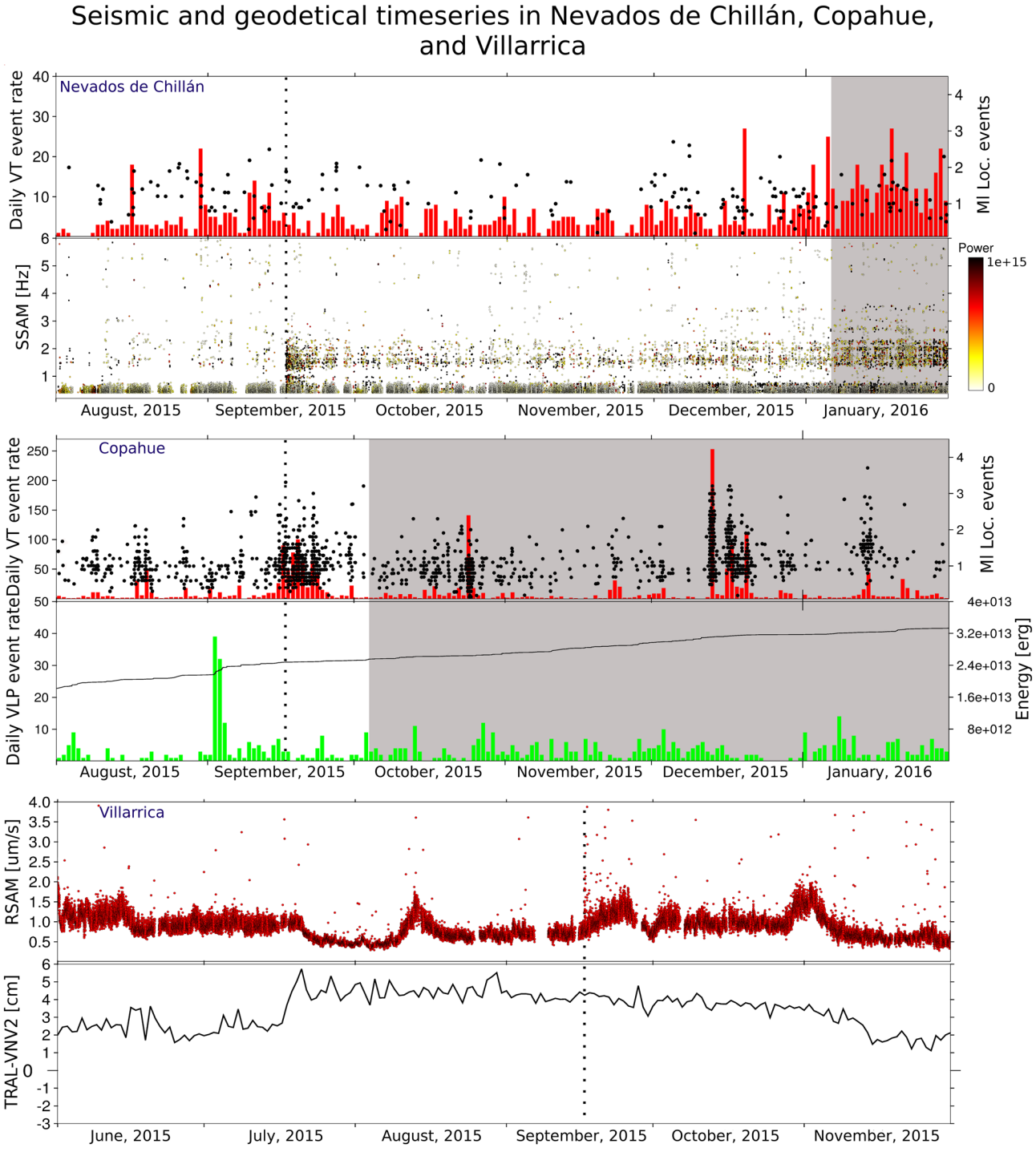

Figure 2. Observations by OVDAS on Nevados de Chillán (NdC), Copahue (COP), and Villarrica (VIL), from 1 August 2015 to 31 January 2016 (NdC and COP), and from 1 June 2015 to 31 December 2016 (VIL). Illapel earthquake occurrence is marked with a dotted line. First and second panels show the daily VT event rate in red bars (with the magnitude of the larger events in a day in black dots) and the SSAM, for NdC. The first week of the SSAM record may contain some contamination from the aftershock signals of the Illapel earthquake. Third and fourth panels show the daily VT event rate (and magnitude of the larger earthquakes) and the daily VLP event rate (with the cumulative released energy) for COP. Fifth and sixth panels show the RSAM and the difference of the position of the TRA and VN2 GPS stations for Villarrica. Gray regions highlight the eruptive phases of NdC and COP, which started on 6 January 2016 and 3 October 2015, respectively.

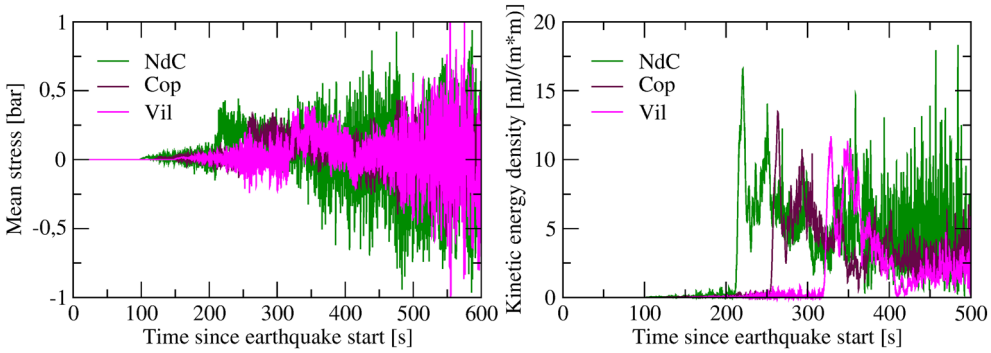

Figure 3. Left panel: Dynamic variations on mean stress due to the 2015 M_W 8.3 Illapel earthquake at Nevados de Chillán (NdC), Copahue (COP), and Villarrica (VIL) volcanoes during the first 600 s that followed the megathrust, which is where the larger variations occur. Right panel: Dynamic variations on kinetic energy density, due to the same earthquake, during the first 500 s that followed the mainshock occurrence.

by mild degassing, in January 2016. The lack of a correlation between the beginning of the unrest and the timing of the earthquake does not allow us to link it to the influence of the Illapel earthquake: This increase in the number of LP events seems more likely to be related to the natural activity of the volcano, which has had several periods of phreatic activity and seismic unrest since 2010. Another volcano that had a period of unrest after the earthquake was Láscar, in North Chile. Phreatic explosions were registered in October, which have been linked to the occurrence of heavy rains and not the earthquake (Gaete et al., 2020).

3.3. Influence of the Illapel Earthquake

The most prominent impact of the earthquake comes from the surface waves (Farías et al., 2014; Fuchs et al., 2014; Hill et al., 2002; Jay et al., 2011; Manga & Brodsky, 2006). In our case Rayleigh waves have a period of about 20 s, so they still have an important amplitude at a depth of 3 km (Stein & Wysession, 2003). Figure 3 shows the waveforms with the maximum variations in the mean stress and the kinetic energy density, at the reservoir of each volcanic system. Peak values of mean stress are relevant, in the order of 0.5–1 bar, which means that the earthquake could have affected the dynamics of the hydrothermal fluids during the shaking. The values of peak kinetic energy density in the volcanoes are in the order of 12–17 mJ/m^2, which are high enough to induce hydrothermal responses (Wang & Manga, 2010).

We calculated the differences in displacement between points located at both sides of the faults (Figure 4) when the amplitude of the shaking is the largest and computed them both normal and parallel to the fault line. Displacement differences normal to the structures tell us whether we have clamping (negative values) or unclamping (positive values) at them, and differences in the displacement parallel to a certain fault line tell us about the shearing induced by the earthquake at the structure. Here we are considering that some of these faults might be related to preexisting magma pathways. The earthquake is promoting clamping at these structures and the parallel component of the displacement difference shows an important left-lateral, strike-slip motion at them. For NdC, this motion induced in the main NW trending structure is large enough to induce a permanent increase in permeability beneath the volcano (Pérez-Flores et al., 2017). Past works have linked this NW fault as one of the main pathways to move and store fluids (Farías & Galván, 2020; Farías et al., 2014). In COP we can see two interesting behaviors: The main fault, which is the northernmost section of the LOFS, is activated with left-lateral strike-slip motion near the proposed fluid reservoir. The second behavior occurs at the northern in the border of the Caviahue caldera, where there is a transition between the LOFS and a N-NNE fault that has been proposed in the literature (Bonali et al., 2016; Melnick et al., 2006). Right at the transition we have a north trending fault section, where the earthquake promoted mostly clamping (see S1 trace in Figure 4). Nevertheless, as we go toward the south, the left-lateral induced motion becomes relevant, in particular near S2 and S3 points, which correspond to the northern sections of the LOFS. This effect, which occurs because of the fault geometry, generates a temporal transtensional regime in the transition between the two fault systems, which is where the 17 day long VT swarm occurred right after the earthquake (Figure S9). Villarica volcano, the farest of the three to the

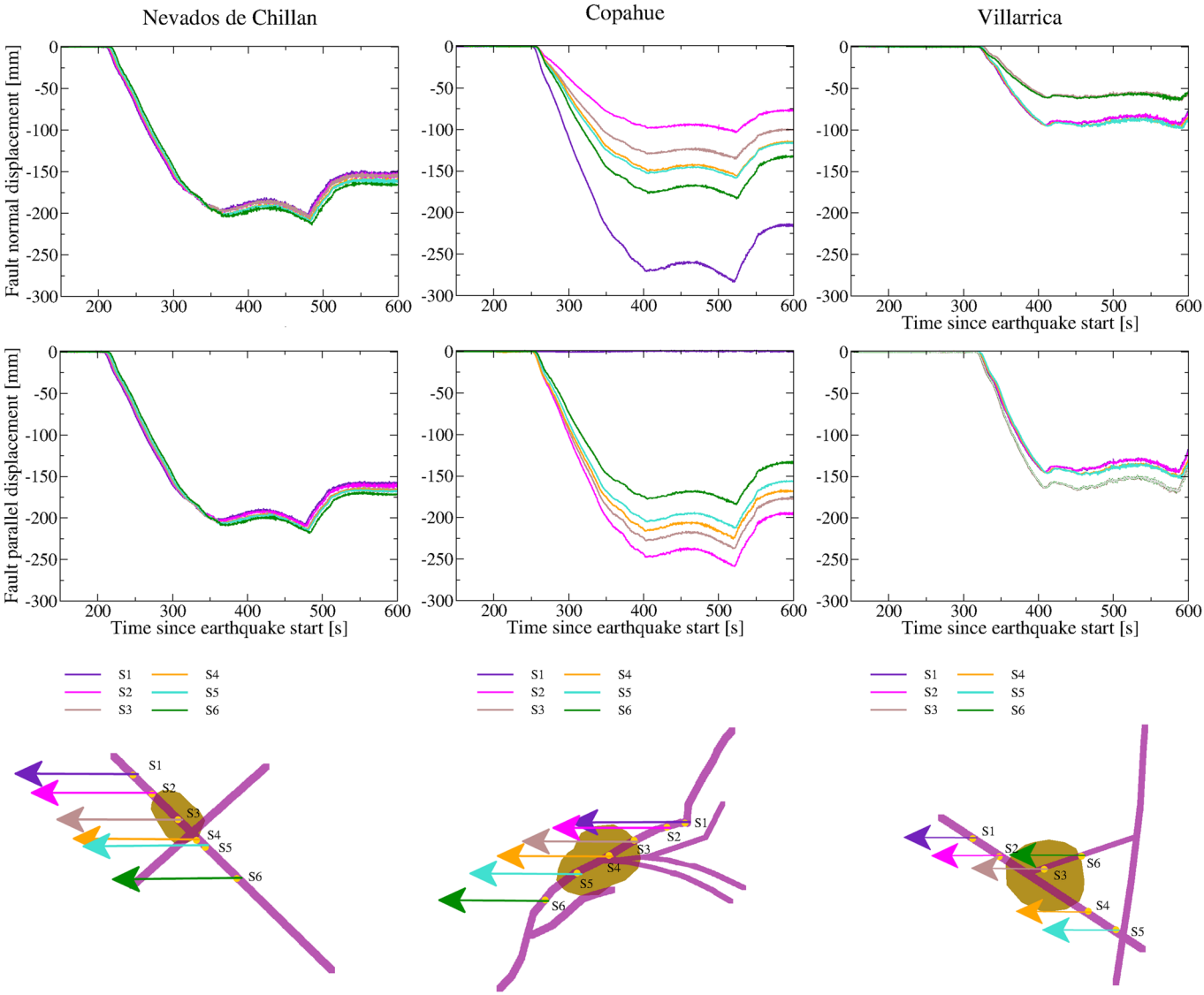

Figure 4. Top panels, from left to right: Variations on displacement normal to a fault at several points of Nevados de Chillán (NdC), Copahue (COP), and Villarrica (VIL) volcanoes. They are calculated around the S points marked in the bottom panels of the figure. Middle panels, from left to right: Variations on displacement parallel to the fault lines. Negative values reflect left-lateral motion, and positive values right-lateral motion, respectively. Bottom panels: Sketch of the main faults and reservoirs used in the simulations (in purple and light brown, respectively), with the location of all the S points, and the maximum variations on displacement sketched as vectors. Vector colors represent the S point at which they are measured, and their sizes are scaled. At NdC, all these points are located in a NW fault, while all S points in COP are emplaced in the NE-NNE faults. Finally, at VIL the S2 and S4 points are located in a NE fault, while all the others are on top of the larger NW fault.

Illapel rupture zone, sits in a complex system of faults. Clamping is the lowest of the three volcanoes because of this, but the left-lateral motion induced is still considerable, in particular in the NE trending fault, which we suggest it can be related to fluid motion since it follows the alignment of several secondary cones of the volcano. Therefore, the increment in permeability due to the transient shearing could have been larger at this structure, which the fluids might have later used to mobilize.

4. Discussion and Conclusions

Our results show that even at large distances an earthquake can significantly affect active volcanic systems. This is a well-known phenomenon (Bebbington & Marzocchi, 2011; Delle Donne et al., 2010; Eggert & Walter, 2009; Linde & Sacks, 1998; Sawi & Manga, 2019; Walter & Amelung, 2007), but this case is

special, as the 2015 M_W 8.3 Illapel earthquake affected three volcanoes (NdC, COP, and VIL) in very different ways, with unexpected consequences. In the short term, the earthquake induced important peak dynamic stress changes in the order of 0.5–1 bar at each volcano, which were not strong enough to break the rock at 3 km depth but were large enough induce shearing at certain faults at the volcanoes, that likely increased the permeability, thus allowing high-pressurized fluids to move afterward. This led to an immediate response of these systems, which were already in an altered state before the mainshock.

Nevertheless, the dynamics of each volcano in the weeks and months following the Illapel mainshock were different, although they were related to the earthquake impact on them. In the case of NdC, the influence of the Illapel event at the main NW fault was large, and the motion it induced on the structure likely increased the permeability, which helped hydrothermal fluids to mobilize. A couple of months later, the first phreatic explosions began at the volcano, which likely opened spaces so the magma could arise. This happened later though, when a fissure was opened on top of the active crater, almost two years after the eruption started. At COP, the earthquake created an unexpected transient transtensional regime at the NE border of the Caviahue caldera, in the same place where a VT swarm was recorded afterward. The seismic waves also induced a left-lateral motion at the LOFS, which could have increased permeability at the hydrothermal system. These two combined effects likely destabilized the volcanic system, which entered in a new eruptive phase 17 days after the 2015 Illapel earthquake. Finally, the seismic waves also affected VIL volcano. The short-term response consisted in an increase in seismicity, which was most likely due to the combination of an increase in permeability and a hydrological response mechanism during the passage of the seismic waves. The long-term response from the volcano was a deflation process, which could have been related to the earthquake via a topographic resonance mechanism with the volcanic edifice (Namiki et al., 2019), where the lateral motions from the very low frequency surface waves were very important. This might have induced lateral magma motion, and even a descent, afterward, thus calming the volcano, which then entered in an stable phase. This lateral fluid motion has been suggested in the past in the CSCVZ (Pritchard et al., 2013). It is worth noticing that this long-term response has been rarely seen in literature (Namiki et al., 2019; Sánchez & McNutt, 2004).

Overall, these three very different responses, as such large distances from the earthquake rupture zone, point out to the very complex mechanisms on which an event such as the Illapel megathrust can affect volcanic systems. It also has important implications about the sensitivity of a volcano toward an external perturbation, where both the preseismic state of each one and the geometry of their fault systems can help us to understand why they do or do not respond to an external earthquake.

Data Availability Statement

All geophysical data from OVDAS belongs to the state of Chile and is open to all, but contacting the officer in charge of data access (Fernando Gil Cruz, email:fernando.gil@sernageomin.cl) is a requirement, in accordance to the law N 20285 on the access to public information, promulgated on 11 August 2008. All codes needed to perform the numerical simulations can be found at the following DOI: 10.17605/OSF.IO/3X47G. For instructions on how to use the codes, researchers can contact the corresponding author, Dr. Cristian Farías.

Acknowledgments

This work was funded by the UCT projects "¿Cómo afectan los terremotos externos a la actividad volcánica en Chile?" (VIP 2016PF-CF-08) and "HPC-Cluster UCT: Una iniciativa Interfacultades para el fortalecimiento de la investigacin, vinculacin con el medio, y creacin de redes de forma interdisciplinarias" (VIP FEQUIP2019-INRN-03). The authors want to thank Pablo Gonzalez and Jonathan Lazo, from OVDAS, for the figures of the volcanic parameters he modified, and Drs. Inés Rodriguez and Elisa Ramírez, for useful discussions. The authors are also very grateful with OVDAS-Sernageomin for the seismic data of the volcanic activity.

References

Aki, K. (1981). Deep volcanic tremor and magma ascent mechanism under Kilauea, Hawaii. *Journal of Geophysical Research*, *86*, 7095–7109.

Bachmann, C. E., Wiemer, S., Goertz-Allmann, B. P., & Woessner, J. (2012). Influence of pore pressure on the event size distribution of induced earthquakes. *Geophysical Research Letters*, *39*, L09302. https://doi.org/10.1029/2012GL051480

Bebbington, M. S., & Marzocchi, W. (2011). Stochastic models for earthquake triggering of volcanic eruptions. *Journal of Geophysical Research*, *116*, B05204. https://doi.org/10.1029/2010JB008114

Bizzarri, A. (2012). Rupture speed and slip velocity: What can we learn from simulated earthquakes? *Earth and Planetary Science Letters*, *317-318*, 196–203.

Bonali, F. L. (2013). Earthquake-induced static stress change on magma pathway in promoting the 2012 Copahue eruption. *Tectonophysics*, *608*, 127–137.

Bonali, F. L., Corazzato, C., Belloti, F., & Groppelli, G. (2016). Active Tectonics and its Interactions with Copahue volcano. In F. Tassi, O. Vaselli, & A. T. Caselli (Eds.), *Copahue volcano, active volcanoes of the world* (pp. 23–45). Heidelberg: Springer-Verlag.

Bonali, F. L., Tibaldi, A., Corazzato, C., Tormey, D. R., & Lara, L. E. (2013). Quantifying the effect of large earthquakes in promoting eruptions due to stress changes on magma pathway: The Chile case. *Tectonophysics*, *583*, 54–67.

Cardona, C., Tassara, A., Gil-Cruz, F., Lara, L., Morales, M., Kohler, P., & Franco, L. (2018). Crustal seismicity associated to rapid surface uplift at Laguna del Maule Volcanic Complex, Southern Volcanic Zone of the Andes. *Journal of Volcanology and Geothermal Research*, *353*, 83–94.

Catalán, N., Bataille, K., & Araya, R. (2017). Depth dependent geometry of the LiquiñeOfqui Fault Zone and its relation to paths of slab derived fluids. *Geophysical Research Letters*, *44*, 10,916–10,920. https://doi.org/10.1002/2017GL074870

Cembrano, J., Hervé, F., & Lavenu, A. (1996). The Liquiñe Ofqui fault zone: A long-lived intra-arc fault system in southern Chile. *Tectonophysics*, *259*, 55–66.

Cembrano, J., & Lara, L. (2009). The link between volcanism and tectonics in the southern volcanic zone of the Chilean Andes: A review. *Tectonophysics*, *471*, 96–113.

Córdova, L., Alarcón, A., Mardones, C., Cardona, C., Gil, F., Rojas, G., et al. (2015). Monitoreo de la deformación en volcanes chilenos mediante técnica GPS, resultados asociados a la actividad de los volcanes Laguna del Maule, Copahue y Villarrica. In *XIV Congreso Geológico Chileno*.

Delle Donne, D., Harris, A., Ripepe, M., & Wright, R. (2010). Earthquake-induced thermal anomalies at active volcanoes. *Geology*, *38*, 771–774.

Eggert, S., & Walter, T. (2009). Volcanic activity before and after large tectonic earthquakes: Observations and statistical significance. *Tectonophysics*, *471*, 14–26.

Endo, E., & Murray, T. (1991). Real-time Seismic Amplitude Measurement (RSAM): A volcano monitoring and prediction tool. *Bulletin of Volcanology*, *53*, 533–545.

Farías, C., & Galván, B. (2020). Numerical wave propagation study of the unusual response of Nevados de Chillán volcano to two aftershocks of the 2010 Mw=8.8 Maule earthquake. *Journal of Volcanology and Geothermal Research*, *389*, 106,735.

Farías, C., Galván, B., & Miller, S. A. (2017). Numerical simulations (2D) on the influence of pre-existing local structures and seismic source characteristics in earthquake-volcano interactions. *Journal of Volcanology and Geothermal Research*, *343*, 192–210.

Farías, C., Lupi, M., Fuchs, F., & Miller, S. A. (2014). Seismic activity of the Nevados de Chillán volcanic complex after the 2010 Mw8.8 Maule, Chile, earthquake. *Journal of Volcanology and Geothermal Research*, *283*, 116–126.

Fuchs, F., Lupi, M., & Miller, S. A. (2014). Remotely triggered nonvolcanic tremor in Sumbawa, Indonesia. *Geophysical Research Letters*, *41*, 4185–4193. https://doi.org/10.1002/2014GL060312

Gaete, A., Walter, T. R., Bredemeyer, S., Zimmer, M., Kujawal, C., Franco, L., et al. (2020). Processes culminating in the 2015 phreatic explosion at Lascar volcano, Chile, evidenced by multiparametric data. *Natural Hazards and Earth System Sciences*, *20*, 377–397.

Gonzalez-Ferrán, O. (1995). *Volcanes de Chile*. Chile: Instituto Geográfico Militar.

Heidarzadeh, M., Murotani, S., Satake, K., Ishibe, T., & Gusman, A. (2015). Source model of the 16 September 2015 Illapel, Chile, Mw 8.4 earthquake based on teleseismic and tsunami data. *Geophysical Research Letters*, *43*, 643–650. https://doi.org/10.1002/2015GL067297

Hill, D., Pollitz, P., & Newhall, C. (2002). Earthquake-volcano interactions. *Physics Today*, *55*, 41–47.

Jay, J. A., Pritchard, M. E., West, M., Christensen, D., Haney, M., Minaya, E., et al. (2011). Shallow seismicity, triggered seismicity, and ambient noise tomography at the long-dormant Uturuncu Volcano, Bolivia. *Bulletin of Volcanology*, *74*, 817–837.

Johnson, J., & Palma, J. L. (2015). Lahar infrasound associated with Volcán Villarrica's 3 March 2015 eruption. *Geophysical Research Letters*, *42*, 6324–6331. https://doi.org/10.1002/2015GL065024

Kumagai, H., & Chouet, B. A. (1999). The complex frequencies of long-period seismic events as probes of fluid composition beneath volcanoes. *Geophysical Journal International*, *138*, F7–F12.

Legrand, D., Barrientos, S., Bataille, K., Cembrano, J., & Pavez, A. (2011). The fluid-driven tectonic swarm of Aysen Fjord, Chile (2007) associated with two earthquakes (Mw=6.1 and Mw=6.2) within the Liquie-Ofqui Fault Zone. *Continental Shelf Research*, *31*, 154–161.

Linde, A., & Sacks, I. S. (1998). Triggering of volcanic eruptions. *Nature*, *395*, 888–890.

Luengo, N., Romero, J., Basualto, D., Palma, J., & Lara, L. (2017). Actividad explosiva 2016-2017 del Complejo Volcánico Nevados de Chillán, Región de Ñuble, Chile: Eventos Freáticos o Freatomagmáticos? In *XIII Encuentro Nacional de Estudiantes de Geología*.

Manga, M., & Brodsky, E. (2006). Seismic triggering of eruptions in the far field: Volcanoes and geysers. *Annual Reviews on Earth and Planetary Sciences*, *34*, 263–291.

Martin, R., Komatisch, D., & Ezziani, A. (2008). An unsplit Convolutional Perfectly Matched Layer improved at grazing incidence for seismic wave propagation in poroelastic media. *Geophysics*, *73*, T51–T61.

McNutt, S. (2005). Volcanic seismology. *Annual Reviews on Earth and Planetary Sciences*, *32*, 461–491.

Melnick, D., Folguera, A., & Ramos, V. (2006). Structural control on arc volcanism: The Caviahue-Copahue complex, Central to Patagonian Andes transition (38°S). *Journal of South American Sciences*, *22*, 66–88.

Métois, M., Socquet, A., & Vigny, C. (2012). Interseismic coupling, segmentation and mechanical behavior of the central Chile subduction zone. *Journal of Geophysical Research*, *117*, B03406. https://doi.org/10.1029/2011jb008736

Meulle-Stef, M., Tassara, A., & Pérez-Flores, P. (2016). Stress field and structural model of Nevados de Chillán Volcanic Complex. In *Cities on Volcanoes 9*.

Moreno, H., & Clavero, J. (2006). Mapa Geológico del área del volcán Villarrica.

Namiki, A., Rivalta, E., Woith, H., Willey, T., Parolai, S., & Walter, T. R. (2019). Volcanic activities triggered or inhibited by resonance of volcanic edifices to large earthquakes. *Geology*, *47*, 67–70.

OVDAS-Sernageomin (2015). Reporte Especial de Actividad Volcánica (REAV), Región del Bío-Bío, Año 2015 Septiembre 16 20:45 HL: Servicio Nacional de Geologia y Mineria. https://sitiohistorico.sernageomin.cl/reportesVolcanes/20150916091337484REAV_BioBio_2015-09-16_Copahue.pdf

OVDAS-Sernageomin (2017). Reporte de Actividad Volcánica N°24, Diciembre de 2017, Región del Bío-Bío: Sernageomin.

OVDAS-Sernageomin (2018). Reporte Especial de Actividad Volcánica (REAV), Región del Bío-Bío, 2 de Febrero de 2018, 16:30 Horas (Hora Local): Sernageomin.

OVDAS-Sernageomin (2019). Reporte de Actividad Volcánica (RAV): Sernageomin.

Okada, Y. (1992). Internal deformation due to shear and tensile faults in a half space. *Bulletin of the Seismological Society of America*, *82*, 1018–1040.

Pérez-Flores, P., Wang, G., Mitchell, T. M., Meredith, P. G., Narae, Y., Sarkarf, V., & Cembrano, J. (2017). The effect of offset on fracture permeability of rocks from the Southern Andes Volcanic Zone, Chile. *Journal of Structural Geology*, *104*, 142–158.

Pritchard, M. E., Jay, J. A., Aron, F., Henderson, S. T., & Lara, L. E. (2013). Subsidence at southern Andes volcanoes induced by the 2010 Maule, Chile earthquake. *Nature Geoscience*, *6*, 632–636.

Rogers, J. A., & Stephens, C. D. (1995). The seismic sequence of the 16 September 2015 Mw 8.3 Illapel, Chile, earthquake. *Bulletin of the Seismological Society of America*, *85*(2), 632–639.

Ruiz, S., Klein, E., del Campo, F., Rivera, E., Poli, P., Métois, M., et al. (2016). The seismic sequence of the 16 September 2015 Mw 8.3 Illapel, Chile, Earthquake. *Seismological Research Letters*, *87*(4), 789–799.
Ruiz, S., & Madariaga, R. (2018). Historical and recent large megathrust earthquakes in Chile. *Tectonophysics*, *733*, 37–56.
Sánchez, J., & McNutt, S. (2004). Intermediate-term declines in seismicity at Mt. Wrangell and Mt. Veniaminof volcanoes, Alaska, following the 3 November 2002 Mw 7.9 Denali Fault Earthquake. *Bulletin of the Seismological Society of America*, *94*(6B), S370–S383.
Sánchez, P., Pérez-Flores, P., Arancibia, G., Cembrano, J., & Reich, M. (2013). Crustal deformation effects on the chemical evolution of geothermal systems: The intra-arc LiquiñeOfqui fault system, Southern Andes. *International Geology Review*, *55*, 1384–1400.
Satake, K., & Heidarzadeh, M. (2017). A review of source models of the 2015 Illapel, Chile earthquake and insights from tsunami data. *Pure and Applied Geophysics*, *174*, 1–9.
Sawi, T. M., & Manga, M. (2019). Revisiting short-term earthquake triggered volcanism. *Bulletin of Volcanology*, *80*, 57.
Stanton-Yonge, A., Griffith, W. A., Cembrano, J., Julien, R., & Iturrieta, P. (2016). Tectonic role of margin-parallel and margin-transverse faults during oblique subduction in the Southern Volcanic Zone of the Andes: Insights from Boundary Element Modeling. *Tectonics*, *35*, 1990–2013. https://doi.org/10.1002/2016TC004226
Stein, S., & Wysession, M. (2003). *An introduction to seismology, earthquakes, and Earth structure*: Blackwell publishing.
Tardani, D., Reich, M., Roulleau, E., Takahata, N., Sano, Y., Pérez-Flores, P., et al. (2016). Exploring the structural controls on helium, nitrogen and carbon isotope signatures in hydrothermal fluids along an intra-arc fault system. *Geochimica et Cosmochimica Acta*, *184*, 193–211.
USGS (2015). https://earthquake.usgs.gov/earthquakes/eventpage/us20003k7a. United States Geological Survey.
Venzke, E. S. I. (2020). Global volcanism program. Volcanoes of the world, v. 4.4.1.
Walter, T. (2007). How a tectonic earthquake may wake up volcanoes: Stress transfer during the 1996 earthquake-eruption sequence at the Karymsky Volcanic Group, Kamchatka. *Earth and Planetary Science Letters*, *264*, 347–359.
Walter, T., & Amelung, F. (2007). Volcanic eruptions following M≥9 megathrust earthquakes: Implications for the Sumatra-Andaman volcanoes. *Geology*, *35*, 539–542.
Wang, C. Y., & Manga, M. (2010). Hydrologic responses to earthquakes and a general metric. *Geofluids*, *10*, 206–216.
Wassermann, J. (2012). *Volcano Seismology, IASPEI New Manual of seismological observatory practice 2*. Potsdam: Deutsches GeoForschungsZentrum GFZ.
Watt, S., Pyle, D., & Mather, T. (2009). The influence of great earthquakes on volcanic eruption rate along the Chilean subduction zone. *Earth and Planetary Science Letters*, *277*, 399–407.